

Energy Management and Control System for Laboratory Scale Microgrid based Wind-PV-Battery

Adel Merabet, *Member, IEEE*, Khandker Tawfique Ahmed, *Member, IEEE*, Hussein Ibrahim, Rachid Beguenane, *Member, IEEE* and Amer Ghias, *Member, IEEE*

Abstract—This paper proposes an energy management and control system for laboratory scale microgrid based on hybrid energy resources such as wind, solar and battery. Power converters and control algorithms have been used along with dedicated energy resources for the efficient operation of the microgrid. The control algorithms are developed to provide power compatibility and energy management between different resources in the microgrid. It provides stable operation of the control in all microgrid subsystems under various power generation and load conditions. The proposed microgrid, based on hybrid energy resources, operates in autonomous mode and has an open architecture platform for testing multiple different control configurations. Real-time control system has been used to operate and validate the hybrid resources in the microgrid experimentally. The proposed laboratory scale microgrid can be used as a benchmark for future research in smart grid applications.

Index Terms-- Wind energy, solar energy, conversion, storage, hybrid system, control, energy management.

I. INTRODUCTION

DISTRIBUTED energy generation systems based on renewable energy sources, such as solar photovoltaic (PV) and wind energy are playing a major role in the clean energy production. Due to the intermittence of the solar and wind energy, energy storage system (ESS) is integrated to provide sustainable energy, especially, when operating in standalone mode. Such hybrid energy system requires multiple control strategies to ensure smooth and efficient power transfer [1], [2].

The microgrid configuration depends on the type of power

converters used in between different energy sources and the loads. Typically AC-DC, DC-AC and DC-DC converters are integrated in the distributed energy system due to the different natures of the output voltages. Such configurations involve critical technical issues, which has attracted significant research attention [3]–[6]. Simulation based validation in microgrid has been conducted to verify the supervisory, management and control system [7]–[9]. Some experimental work was also validated through test-beds of fixed configuration in [10]–[12]. A configurable based architecture, that is flexible and can be used to validate advanced control algorithms in a real time environment and test microgrids at laboratory scale. Thus, it can be used for educational and research purposes.

An autonomous operation of the microgrid, through controlling the distributed sources power, will enhance the performance of the microgrid. This smart system can be achieved by an energy management and control system, operating to supervise the power flow in the microgrid [13].

The objective of this paper is to develop and design a laboratory scale stand-alone microgrid that utilizes hybrid energy resources such as wind, PV and battery energy storage. The energy between these different resources is managed using control algorithms that are used in the real-time control environment. The proposed system has many capabilities to perform experimental research and studies in the field of renewable energy. It has an open architecture structure, where different power electronics converter configurations and control algorithms can be implemented and tested to evaluate the microgrid performance. The experimental renewable energy test-bed includes three major parts:

- 1- Renewable energy sources (wind turbine based permanent magnet synchronous generator (PMSG) and PV module) with their appropriate power electronics converters, battery based energy storage system (ESS), and single phase AC load. These components are connected through a DC-link as shown in Fig. 1.
- 2- Real time supervisory and control system using a real-time digital simulator and a data acquisition interface.
- 3- Energy management and control system software for the microgrid operation as a smart system.

Manuscript received February 11, 2016; revised May 21, 2016; accepted June 24, 2016. This work was supported in part by the Canada Foundation for Innovation project 30527 and the Natural Sciences and Engineering Research Council of Canada (NSERC) under Engage Grant EGP 469636-14. Paper no. TSTE-00272-2016.

Adel Merabet and Khandker Tawfique Ahmed are with the Division of Engineering, Saint Mary's University, Halifax, NS B3H 3C3 Canada (corresponding author phone: 902-420-5712; fax: 902-420-5021; e-mail: adel.merabet@smu.ca).

Hussein Ibrahim is with TechnoCentre éolien, Gaspé, QC, Canada (e-mail: hibrahm@eolien.qc.ca)

Rachid Beguenane is with the Department of Electrical Engineering, Royal Military College, Kingston, ON, Canada (e-mail: rachid.beguenane@rmc.ca)

Amer Ghias is with the Department of Electrical Engineering, University of Sharjah, Sharjah, United Arab Emirates (e-mail: aghias@sharjah.ac.ae)

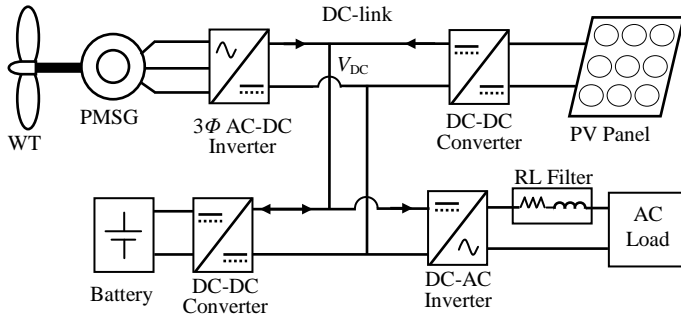


Fig. 1. Components of the laboratory scale experimental microgrid

The proposed laboratory scale microgrid is operated as a smart system by an energy management and control system. The PV system is controlled to run under maximum power point tracking (MPPT) under low energy generation and off-MPPT during excess of energy to meet the load requirement. The wind energy conversion system (WECS) is controlled by a feedback control law, for speed tracking, enhanced by a disturbance compensator to reject unknown turbine torque. An energy management algorithm, taking into consideration the available power from the renewable sources, the load power demand and the state of the battery, is developed to operate the microgrid as an autonomous system. Finally, the voltage at the load side is regulated to ensure efficient power transfer from the energy sources to the load.

II. PV ENERGY CONVERSION SYSTEM

The PV energy conversion system includes a PV module and a DC-DC boost converter. Depending on the state of the storage system, which it will be discussed in the energy management section, it can be operated under maximum power point tracking (MPPT) for maximum power extraction or off-MPPT for power balance as shown in Fig. 2.

The power P_{pv} of the PV panel is expressed as

$$P_{pv} = VI \quad (1)$$

where, V and I are the voltage and current at the terminals of the PV module.

The MPPT algorithm follows the power variation

$$dP_{pv} = dV I + V dI \quad (2)$$

At the maximum power point, the power variation with respect of the voltage is

$$\frac{dP_{pv}}{dV} = I + V \frac{dI}{dV} = 0 \quad (3)$$

For practical implementation, the derivatives have been numerically approximated by the following discretisation method

$$dV(t) \approx \Delta V(k\Delta t) = V(k\Delta t) - V((k-1)\Delta t) \quad (4.a)$$

$$dI(t) \approx \Delta I(k\Delta t) = I(k\Delta t) - I((k-1)\Delta t) \quad (4.b)$$

$$dP_{pv}(t) \approx \Delta P_{pv}(k\Delta t) = \Delta V(k\Delta t) I(k\Delta t) + V(k\Delta t) \Delta I(k\Delta t) \quad (4.c)$$

where, k is a positive integer and Δt is the sampling time.

The MPPT algorithm is detailed in the flowchart of Fig. 3.

How to control the Vdc to constant? By dc-dc converter of the battery

In case of power generation excess and no storage capacity in the battery system, the proposed energy management system switches the PV controller from the MPPT mode to the off-MPPT mode in order to reduce the generated power and maintain a balanced power in the standalone system.

In off-MPPT, the voltage reference is carried out as

$$V_{ref} = \frac{P_L - P_w}{I} \quad (5)$$

where, P_L is the load power and P_w is the power from the wind energy system.

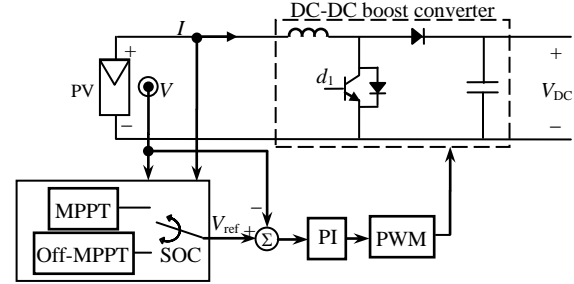


Fig. 2. PV energy conversion system

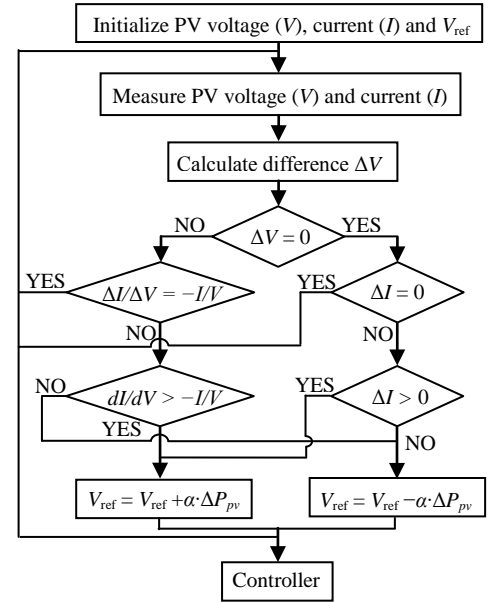


Fig. 3. MPPT algorithm flow chart

III. WIND ENERGY CONVERSION SYSTEM

A. Wind turbine emulation

The wind turbine is emulated by a dynamometer, through the *Turbine Emulator* control function, to reproduce behaviour under the power curve shown in Fig. 4. The *Turbine Emulator* control function set, shown in Fig. 4, is a package of control functions that can be activated in the four-quadrant dynamometer enabling the machine to emulate the operation of a real wind turbine with the power curve of Fig. 4. This function makes the permanent-magnet dc motor of the four-quadrant dynamometer faithfully reproduce the effect of wind on the bladed rotor of a small-scale wind turbine. The torque-speed characteristic at the shaft of the generator coupled to the four-quadrant dynamometer is the same as the one that is obtained when wind blows at a certain speed on

the rotor of the wind turbine. The user has control over the wind speed by changing it through the Wind Speed slider, as shown in Fig. 4.

The speed reference, to be used in the speed control loop, is generated from a look-up table built from the power curve (Fig. 4), to operate under MPPT. In order to avoid abrupt changes in the rotational speed and operate the wind turbine within a safe region, the wind speed profile is passed through a low pass filter (LPF) to eliminate high frequencies due to the sudden speed changes and avoid sudden brief increase in the turbine rotational speed, which causes high peak currents in the generator.

The drive train of the wind turbine is represented as a single lumped mass with the following model [14]

$$\dot{\omega}_r = \frac{1}{J}(T_r - K\omega_r - T_g) \quad (6)$$

where, ω_r is the rotor angular speed, J is the total moment of inertia and K is total damping and T_g is the generator electromagnetic torque.

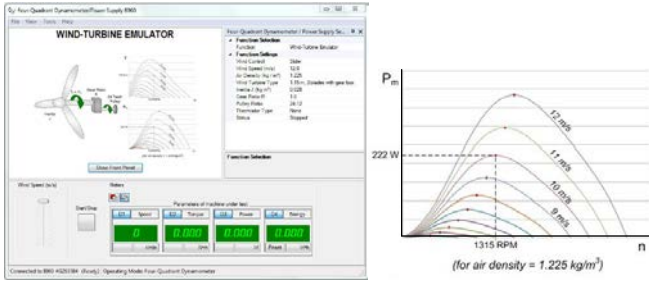


Fig. 4. Wind turbine emulator interface and power curve

B. Permanent Magnet synchronous generator

The three-phase permanent magnet synchronous generator is modelled in the (d, q) reference frame as

$$\begin{cases} \dot{i}_{sd} = -\frac{R}{L_d}i_{sd} + \frac{L_q}{L_d}p\omega_r i_{sq} + \frac{1}{L_d}v_{sd} \\ \dot{i}_{sq} = -\frac{R}{L_q}i_{sq} + \frac{L_d}{L_q}p\omega_r i_{sd} - \frac{1}{L_q}p\omega_r\phi_v + \frac{1}{L_q}v_{sq} \end{cases} \quad (7)$$

where, v_d and v_q are the d - q components of the stator voltage; i_{sd} and i_{sq} are the d - q components of the stator current; ϕ_v is the permanent magnet magnetic flux linkage, R is the stator resistance; L_d and L_q are the stator winding d - q components of the inductance and p is the number of pair poles.

The electromagnetic torque of the generator, by taking into consideration the symmetry in the generator ($L_d = L_q$), is given by

$$T_g = p\phi_v i_{sq} \quad (8)$$

C. Generator side control

The generator side converter control scheme has a cascade structure for operation at maximum power extraction. It includes an outer loop speed controller and an inner loop current control to provide the switching pulses for the AC-DC inverter as shown in Fig. 5.

In this work, model based control strategy has been developed from (6), (7) and (8), by considering the turbine

torque T_r as an unknown disturbance. The proposed speed feedback control law is given by

$$T_g^* = -J(\dot{\omega}_{ref} + k_1 e_{\omega}) - K\omega_r + \left[k_p e_{\omega} + k_i \int e_{\omega} d\tau \right] \quad (9)$$

where ω_{ref} is the speed reference carried out from the MPPT strategy, T_g^* is the controller output, $e_{\omega} = \omega_{ref} - \omega$ is the speed error, and (k_1, k_p, k_i) are the control gains.

The term \hat{T}_r , in (9), represents the compensation of the unknown wind turbine torque and has an integral action, which allows the elimination of the steady state error. This compensation term enhances the controller performance compared to other techniques of feedback control, where the turbine torque is required in the controller implementation [15], [16].

The current feedback control law is given by

$$\begin{cases} v_{sd}^* = L_d(\dot{i}_{dref} + k_e e_d) + R i_{sd} - L_q p\omega_r i_{sq} \\ v_{sq}^* = L_q(\dot{i}_{qref} + k_e e_q) + R i_{sq} - L_d p\omega_r i_{sd} + \phi_v p\omega_r \end{cases} \quad (10)$$

where i_{dref} and i_{qref} are the $(d-q)$ components of the current reference, $e_d = i_{dref} - i_d$ and $e_q = i_{qref} - i_q$ are the $(d-q)$ components of the current tracking error, and v_{sd}^* and v_{sq}^* are the controller outputs.

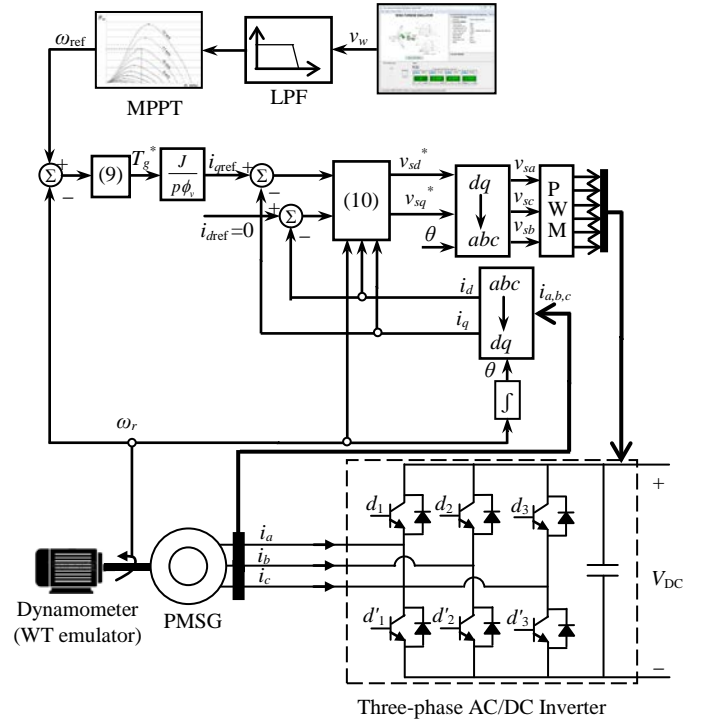


Fig. 5. Generator side converter control scheme of the WECS

IV. ENERGY STORAGE SYSTEM

The energy storage system (ESS) consists of a lead acid battery and a bidirectional DC-DC buck-boost converter connected at the DC-link of the microgrid. The role of this converter is to maintain the DC-link voltage constant despite the power changes in the sources and the load. The DC-link voltage is controlled in the ESS through a PI control cascade strategy as shown in Fig. 8.

Vdc must lower than that of Vbat for this converter topology

An important parameter to represent the state of the battery is the state of charge (SOC) expressed by

$$SOC = 100 \left(1 + \frac{\int I_{bat} dt}{Q} \right) \quad (11)$$

where, I_{bat} is the battery charging current and Q is the battery capacity.

The battery charge-discharge depends on the available power, the demand and the SOC [5]. The energy constraints of the battery are determined based on the SOC limits

$$SOC_{min} \leq SOC \leq SOC_{max} \quad (12)$$

where, SOC_{min} and SOC_{max} are the minimum and the maximum allowable states for the battery safety.

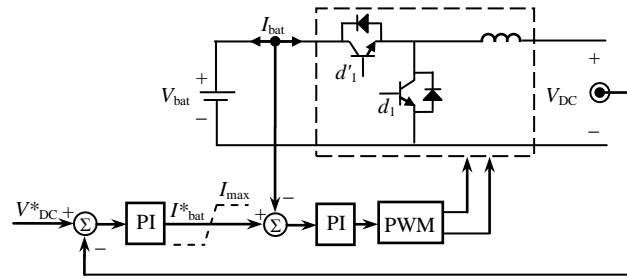


Fig. 6. ESS and control structure

V. ENERGY MANAGEMENT SYSTEM

The energy management system (EMS) coordinates the control of the converters in the hybrid isolated microgrid. The control algorithms for those converters were presented in the previous sections, where the AC-DC converter of the wind turbine generator is controlled to regulate the rotational speed to achieve the wind energy MPPT, the DC-DC converter of the PV system may operate in the MPPT or off-MPPT modes based on the system power balance and energy constraints, and the DC-DC converter of the battery operates either in charging or discharging mode, based on the power balance in the system, in order to maintain a constant DC-link voltage.

The power in the microgrid under various loads and supply conditions should be balanced as follows

How about Q?

$$P_w + P_{pv} - P_{loss} = P_L + P_{bat} \quad (13)$$

where, P_{bat} is the battery power and P_{loss} is the total power loss in the microgrid.

The PV converter operation modes (MPPT, off-MPPT) and the battery converter current flow direction are determined by the energy management system based on the system net power P_{net} and the energy constraints of the battery. The EMS diagram is shown in Fig. 7. If the power, generated by the renewable sources (wind and solar), is insufficient for the demand power at the load side (P_L), it causes a drop in the DC-link voltage V_{DC} . The positive error ($V_{DC}^* - V_{DC}$) produces a positive reference current, which will operate the converter in buck mode to transfer power from the battery to the load (discharge) if its SOC is greater than the minimum value, otherwise load shedding is required to maintain power balance as the power supply is less than

demand and the battery is at its minimum (SOC_{min}). In case of power generation exceeding the load power, DC-link voltage V_{DC} increases, which causes a reference current to control the battery converter in a boost mode (charge), in which power flows from the main DC-link to the battery with the extra generated power, however, if the battery SOC exceeds its maximum (SOC_{max}), the battery charging mode stops and the PV system operates in off-MPPT mode to reduce the generated power in order to balance the power in the microgrid.

V. LOAD SIDE CONTROL

The single phase resistive load is connected to the hybrid energy system through a single phase DC-AC inverter, as shown in Fig. 8, which is controlled to regulate the load side voltage. A resistive-inductive (RL) filter is used to remove the higher order harmonics from the output AC voltage.

The voltage balance through the RL filter is expressed as

$$\dot{i} = -\frac{R}{L}i + \frac{1}{L}(v - v_1) \quad (14)$$

where, v is the voltage at the load side, v_1 is the voltage at the inverter output, i is the current through the filter circuit, R and L are the filter resistance and inductance, respectively.

The load voltage and current are

$$v(t) = V_o \sin(\omega_o t + \phi_v) \quad (15.a)$$

$$i(t) = I_o \sin(\omega_o t + \phi_i) \quad (15.b)$$

where, V_o and I_o are the peak value voltage and current, respectively, (ω_o is the frequency, ϕ_v and ϕ_i are the voltage and current phases, respectively).

A cascade control structure is developed for voltage and current control to regulate the load voltage to be at a constant peak value. In this cascade strategy, the voltage controller (outer loop) compares the RMS voltage to a reference, then, the error is passed through a PI controller to generate the current reference to be used in the current controller (inner loop).

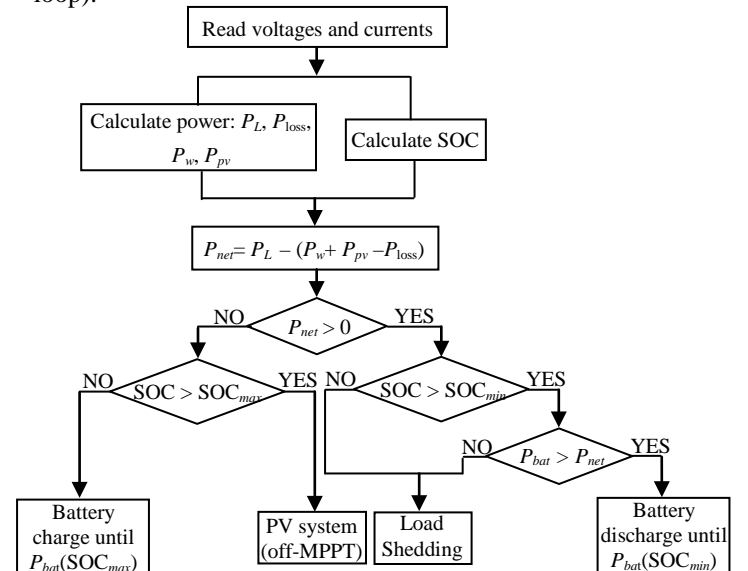


Fig. 7. Energy management system

The diagram illustrates the control system for a single-phase inverter. It is composed of three main functional blocks:

- DC-AC converter:** A four-switch inverter (IGBTs d_1, d_2, d'_1, d'_2) driven by a DC voltage V_{DC} . The inverter's output is connected to an AC load through an $R-L$ filter. The output current is i and the output voltage is v .
- Cascade control:** This block implements a two-loop control strategy. It takes the RMS value of the output voltage v as input. The first loop is a PI controller that generates a reference current I_{ref} based on the difference between the reference current I_{ref} and the measured RMS current I_{RMS} . The second loop is another PI controller that generates a reference voltage V_{ref} based on the difference between the reference voltage V_{ref} and the measured output voltage v . The output of the cascade control is a PWM signal for the inverter.
- Single phase PLL:** This block locks the phase of the output voltage v . It uses an orthogonal system to generate V_α and V_β components. These are transformed into the $d-q$ frame using an $\alpha-\beta$ to $d-q$ block. The d -axis component V_d is compared with its reference $V_{d,ref} = 0$ and the error is processed by a PI controller. The resulting q -axis component V_q is then integrated to produce the phase angle θ . The PLL also outputs the estimated frequency f_o and the RMS value of the voltage V_{RMS} .

VI. REAL TIME MONITORING AND CONTROL INTERFACE

The rapid control prototyping (RCP) of the microgrid based on hybrid wind-PV energy with battery storage and its control system has been conducted using Opal-RT hardware (OP5600 and OP8660) and LabVolt Electromechanical Training System, as shown in Fig. 9. The schematic of the hardware connections between all modules is illustrated in Fig. 10.

The OP5600, real-time digital simulator, consists of analog and digital I/O signal modules, a multi-core processor and FPGA that runs RT-LAB real-time simulation software platform. It enables to conduct a real-time RCP of the controlled microgrid with low time step to achieve the best accuracy. It is equipped with the processor Intel Xeon QuadCore 2.40 GHz, which make it a powerful tool for RCP and hardware-in-the-loop (HIL) applications [19].

B. Real Time Monitoring and Control Software

A real-time software application, for measurement, test and control, is developed in MATLAB/Simulink environment and integrated into RT-LAB for real-time monitoring. RT-LAB is an open real-time simulation software environment capable of performing real-time RCP of the controlled microgrid using the OP5600. In order to execute the model in different target processors, or nodes, it is separated into two subsystems: 1- Console subsystem, which must be identified by the prefix (SC_) in its name (SC_name), is executed in the command station-PC and includes user interface blocks, such as scopes, displays and reference command; 2- Master subsystem, which must be identified by the prefix (SM_) in its name (SM_name), is executed in the CPU core processor of the OP5600 and includes all the computational elements of the model, the mathematical operations of the algorithms and the input-output blocks. As the two subsystems are executed in different targets, or nodes, the communication and synchronization between them is done through the RT-LAB OpComm blocks as shown in Fig. 11.

C. Test-Bed Setup

VII. EXPERIMENTAL RESULTS

1949-3029 (c) 2016 IEEE. Personal use is permitted, but republication/redistribution requires IEEE permission. See http://www.ieee.org/publications_standards/publications/rights/index.html for more information.

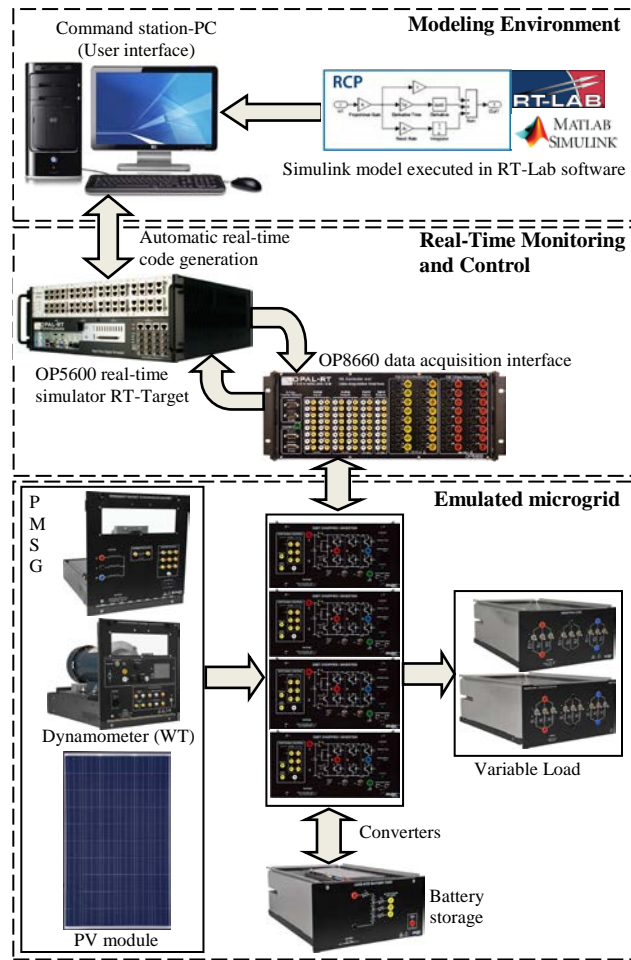


Fig. 9. Rapid control prototyping of the microgrid based hybrid energy sources

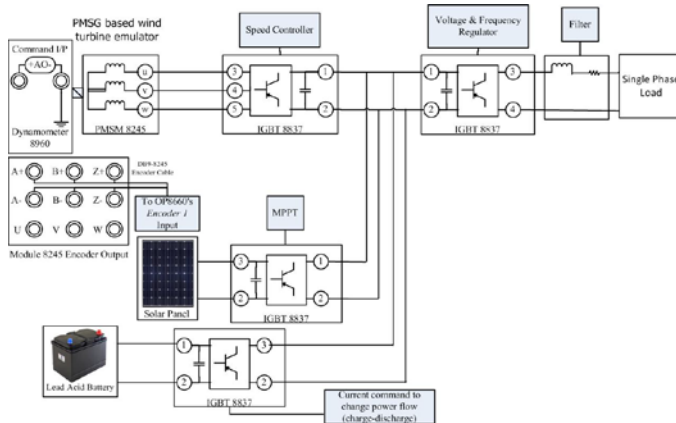


Fig. 10. Hardware connections of the experimental set-up.

In all scenarios, the control gains, provided in table V, were chosen by trial and error and kept constant. The experiment runs to 60 s of time due to the limited memory storage of the host PC. This work is just a preliminary demonstration of the functionality of the proposed microgrid, and long-time experiment will be shown in the future.

First, the experimental microgrid was tested under variable distributed power generation and fixed load. The turbine-generator speed was changed following step variation, as shown in on Fig. 13, by changing the wind speed through the slider, and the PV panel was operated under variable

irradiation by deactivating the lamps at different time instants as shown in the current response of Fig. 14. The resistive load was kept constant. The objective is to provide a constant power to the load regardless the produced power from all sources. The power balance in the system is achieved by maintaining a constant DC-link voltage, which is successfully reached by the proposed control system as observed in Fig. 15 through charging-discharging the battery, as shown in Fig. 16. The power balance in the system can be observed from Fig. 17, where until $t=15s$, the battery is charging as the produced renewable power exceeds the required power by the load, then, discharging process starts as the a drop in wind and solar powers occur in the system. From $t=30s$ to $40s$, the discharge increases with the drop of PV power. After $t=40s$, the battery power discharge decreases as more wind power is added in the system after that instant. During the entire power transfer, the load power is maintained constant as shown in Fig. 17.f. The SOC of the battery is following the charge-discharge process as shown in Fig. 18 and the load voltage is maintained at constant level as shown in Fig. 19.

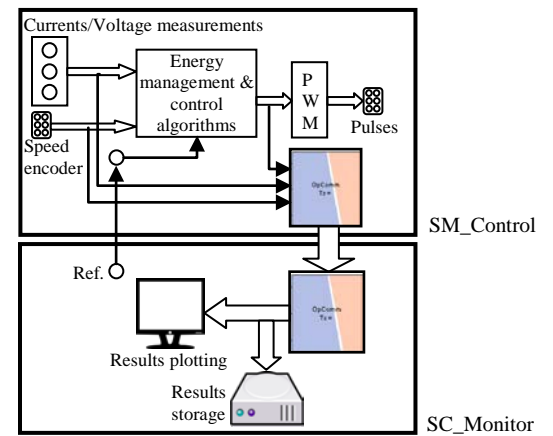


Fig. 11. Subsystems of the model in RT-LAB

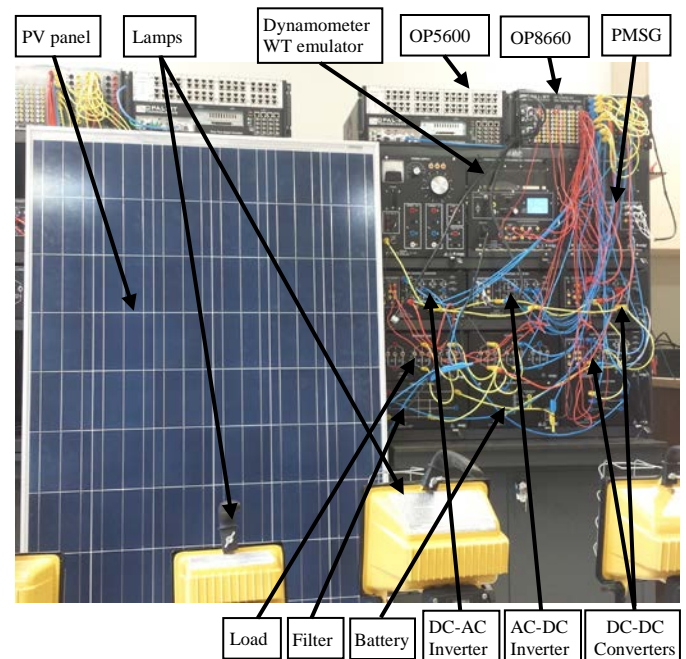


Fig. 12. Experimental microgrid energy system

How about variable generation and variable load demand?

Then, a constant power generation from the wind and PV system and variable load demand was tested as shown in the power responses in Fig. 20. As the load power demand is decreasing until $t = 45$ s, Fig. 20.f, the battery charging is following the profile of that decrease by increasing as shown in Fig. 20.d and 21. After $t = 45$ s, the battery charge decreased, as shown in Fig. 20.d and 21, with the increase of the load power demand. The SOC is increasing with different slopes, as shown in Fig. 22, depending on the load. The DC-link voltage is kept constant, as shown in Fig. 23, during the operation of the microgrid under a variable load. The voltage at the load side is maintained within the limit as shown in Fig. 24.

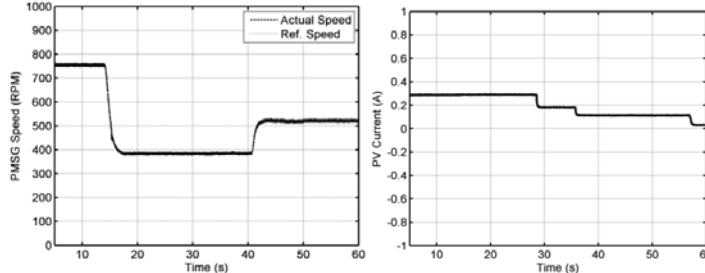


Fig. 13. Wind turbine-generator speed

Fig. 14. PV module current

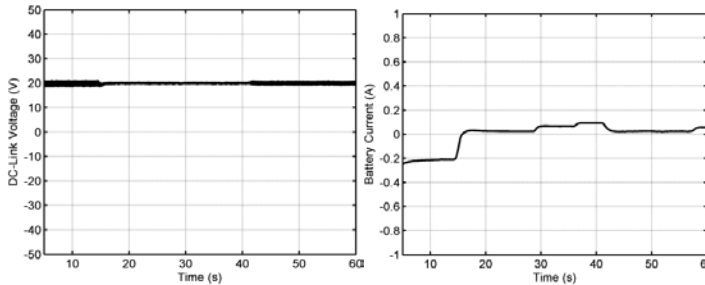


Fig. 15. DC-link voltage

Fig. 16. Battery current

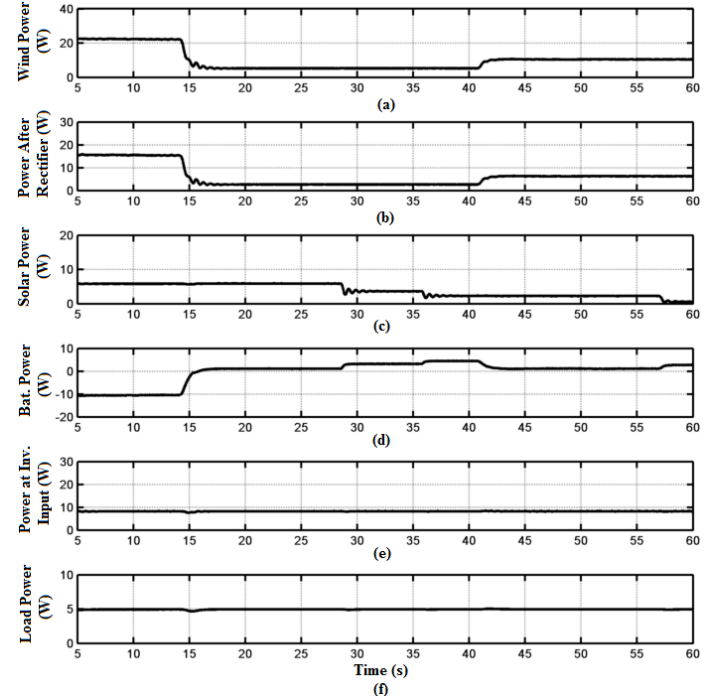


Fig. 17. Power at different locations in the microgrid (variable wind power)

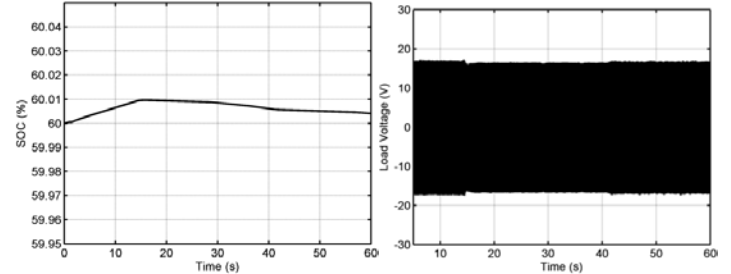


Fig. 18. Battery state of charge

Fig. 19. Load Voltage

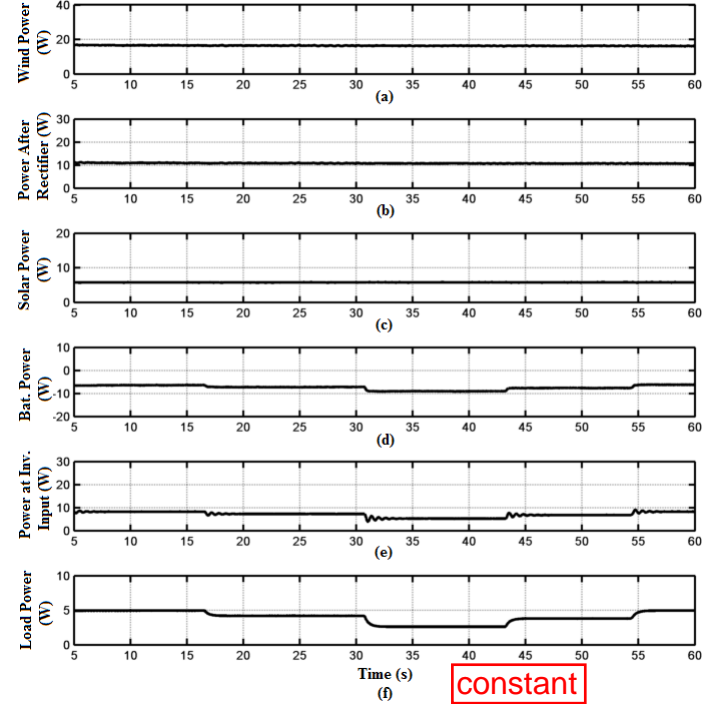


Fig. 20. Power at different locations in the microgrid (variable wind power)

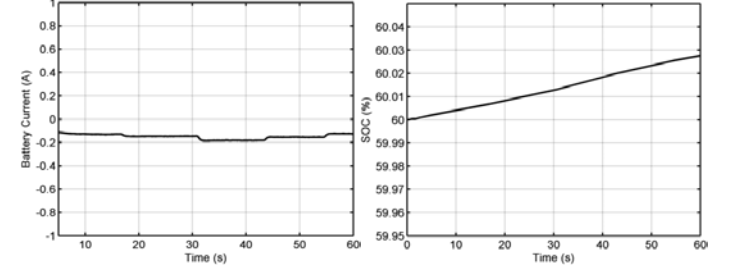


Fig. 21. Battery current

Fig. 22. Battery state of charge

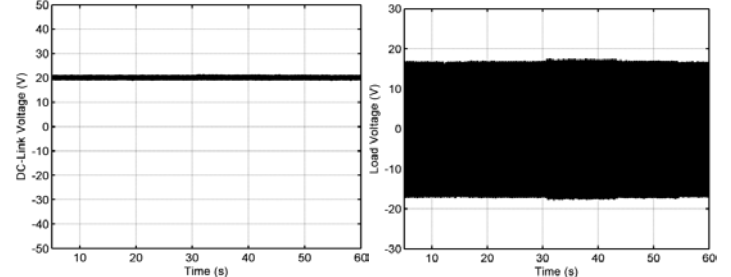


Fig. 23. DC-bus voltage

Fig. 24. Load Voltage

VIII. CONCLUSIONS

A laboratory scale experimental microgrid of distributed renewable energy sources with battery storage and energy management and control system is developed in this paper. The experimental setup is flexible and allows testing

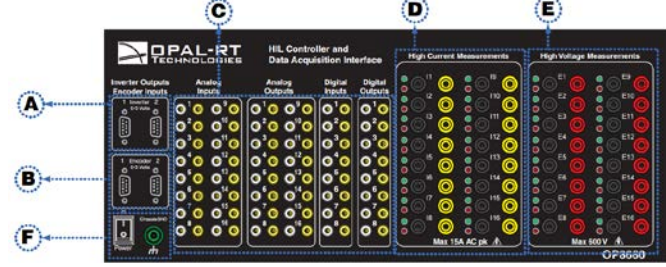
difference power electronics interfaces and combinations. The control software is open source in order to implement different control strategies. This tool contributes to the enhancement of education and research the field of renewable energy and distributed energy systems.

IX. APPENDICES

1. OP5600 Real-Time Digital Simulator

- Powerful real-time target (up to 12 CPU cores, 2.40 GHz)
- Xilinx FPGA
- Real-time OS (Linux Redhat)
- Up to 128 analog I/O or 256 digital I/O or a mix of both
- Distributed parallel computation

2. OP 8660 HIL Controller and Data Acquisition Interface



- A. 6 Pulse Inverter Output connector.
 B. Encoder Input connector used to read motor speed and position using differential ABZ encoder signals.
 C. Analog and digital input/output monitoring connectors for each channel (16 analog or 8 digital).
 D. High current probe connectors (maximum 15 A AC), with red and green LEDs to indicate channel activity.
 E. High voltage probe connectors (maximum 600 V), with red and green LEDs to indicate channel activity.
 F. Power switch and ground connector.

TABLE I

PARAMETERS OF WIND ENERGY CONVERSION SYSTEM

Emulated wind turbine	
Number of blades	3
Air density (kg/m^3)	1.225
Diameter (m)	1.15
Pulley ratio	24:12
Moment of inertia- $J_r(\text{kg}\cdot\text{m}^2)$	0.028
PMSG	
Rated power (W)	260
Rated current (A)	3
Stator resistance- $R_s(\Omega)$	1.3
Stator d-axis inductance- $L_d(\text{mH})$	1.5
Stator q-axis inductance- $L_q(\text{mH})$	1.5
Flux linkage- $\phi_v(\text{Wb})$	0.027
Number of pole pairs- p	3
Moment of inertia- $J_g(\text{kg}\cdot\text{m}^2)$	1.7×10^{-6}
Coefficient of friction- $K_g(\text{Nm}\cdot\text{s/rad})$	0.314×10^{-6}

TABLE II

PARAMETERS OF DC-BUS AND R-L FILTER

DC-bus voltage reference (V)	20
DC-bus capacitor- $C(\text{mF})$	1.8
Filter resistance- $R(\Omega)$	0.5
Filter inductance- $L(\text{mH})$	25

TABLE III

SPECIFICATIONS OF CS6P-260M PV MODULE UNDER STC

Maximum Power (W)	260
Open Circuit Voltage (V)	37.8
Maximum Power Point Voltage (V)	30.7
Short Circuit Current (A)	8.99
Maximum Power Point Current (A)	8.48

TABLE IV
SPECIFICATIONS OF LEAD ACID BATTERY

Type	VRLA
Voltage (A)	48
Capacity (Ah)	10
Maximum Charge Current (A)	4
Maximum Discharge Current (A)	7

TABLE V
CONTROL SYSTEM

Generator side controller (k_i, k_p, k_i)	(0.1, 1, 0.8)
Energy storage system	
Outer loop controller (k_p, k_i)	(0.05, 0.35)
Inner loop controller (k_p, k_i)	(50, 25)
Load side	
Outer loop controller (k_p, k_i)	(20, 1.25)
Inner loop controller (k_p, k_i)	(5, 20)

X. REFERENCES

- [1] A. Bari, J. Jiang, W. Saad and A. Jaekel, "Challenges in the Smart Grid Applications: An Overview," *Int. J. of Distributed Sensor Networks*, pp.1–12, 2014.
- [2] M. B. Shadmand and R. S. Balog, "Multi-objective optimization and design of photovoltaic-wind hybrid system for community smart DC microgrid," *IEEE Trans. Smart Grid*, vol. 5, no. 5, pp. 2635–2643, Sep. 2014.
- [3] M. J. Hossain, H. R. Pota, M. A. Mahmud and M. Aldeen, "Robust control for power Sharing in microgrids with low-inertia wind and PV generators," *IEEE Trans. Sustain. Energy*, vol. 6, no. 3, pp. 1067–1077, Jul. 2015.
- [4] Zaheeruddin and M. Manas, "Renewable energy management through microgrid central controller design: an approach to integrate solar, wind and biomass with battery," *Energy Reports*, vol. 1, pp.156–163, 2015.
- [5] A. Tani, M. B. Camara and B. Dakyo, "Energy management in the decentralized generation systems based on renewable energy—ultracapacitors and battery to compensate the wind/load power fluctuations," *IEEE Trans. Ind. Appl.*, vol. 51, no. 2, pp. 1817–1827, 2015.
- [6] W. Qi, J. Liu, and P. D. Christofides, "Distributed supervisory predictive control of distributed wind and solar energy systems," *IEEE Trans. Control Syst. Technol.*, vol. 21, no. 2, pp. 504–512, 2013.
- [7] X. Li, D. Hui, and X. Lai, "Battery energy storage station (BESS)-based smoothing control of photovoltaic (PV) and wind power generation fluctuations," *IEEE Trans. Sustain. Energy*, vol. 4, no. 2, pp. 464–473, 2013.
- [8] S. Bae, and A. Kwasinski, "Dynamic modeling and operation strategy for a microgrid with wind and photovoltaic resources," *IEEE Trans. Smart Grid*, vol. 3, no. 4, pp. 1867–1876, 2012.
- [9] X. Liu, P. Wang and P. C. Loh, "A Hybrid AC/DC Microgrid and Its Coordination Control," *IEEE Trans. Smart Grid*, vol. 2, no. 2, pp. 278–286, 2011.
- [10] M. Farhadi, O. A. Mohammed, "Design and hardware implementation of laboratory-scale hybrid DC power system for educational purpose," in *Proc.122nd ASEE Annual Conference and Exposition*, Seattle, Washington, USA, 2015.
- [11] V. Salehi, A. Mohamed, A. Mazloomzadeh and O.A. Mohammed, "Laboratory-based smart power system, part I: design and system development," *IEEE Trans. Smart Grid*, vol. 3, no. 3, pp. 1394–1404, 2012.
- [12] V. Salehi, A. Mohamed, A. Mazloomzadeh and O.A. Mohammed, "Laboratory-based smart power system, part II: control, monitoring, and protection," *IEEE Trans. Smart Grid*, vol. 3, no. 3, pp. 1405–1417, 2012.
- [13] T. Wang, D. O'Neill, and H. Kamath, "Dynamic control and optimization of distributed energy resources in a microgrid," *IEEE Trans. Smart Grid*, vol. 6, no. 6, pp. 2884–2894, 2015.
- [14] Y. Yang, K-Tat Mok, S-C Tan, and S.Y.R. Hui, "Nonlinear dynamic power tracking of low-power wind energy conversion system," *IEEE Trans. Power Electron.*, vol. 30, no. 9, pp. 5223–5236, 2015.
- [15] C. Xia, Q. Geng, X. Gu, T. Shi, and Z. Song, "Input-output feedback linearization and speed control of a surface permanent-magnet synchronous wind generator with the boost-chopper converter," *IEEE Trans. Ind. Electron.*, vol. 59, no. 9, pp. 3489–3500, 2012.

- [16] F. Delfino, F. Pampararo, R. Procopio, and M. Rossi, "A feedback linearization control scheme for the integration of wind energy conversion systems into distribution grids," *IEEE Syst. J.*, vol. 6, no. 1, pp. 85–93, 2012.
- [17] M. Ciobotaru, R. Teodorescu, and F. Blaabjerg, "A new single-phase PLL structure based on second order generalized integrator," in *Proc. 37th IEEE Power Electronics Specialists Conf.*, June 18–22, pp. 1–6 2006.
- [18] G. Delille, B. François and G. Malarange, "Dynamic frequency control support by energy storage to reduce the impact of wind and solar generation on isolated power system's inertia," *IEEE Trans. Sustain. Energy*, vol. 3, no. 4, pp. 931–939, 2012.
- [19] *Real-Time HIL/RCP Laboratory*, OPAL-RT Technologies, 2014. [Online]. Available: <http://www.opal-rt.com/new-product/real-time-hilrcp-laboratory>.
- [20] *Turbine Emulator, LabVolt Series, 8968-30*, Festo Didactic, 2015. [Online]. Available: https://www.labvolt.com/downloads/datasheet_50-8968-3_en.pdf



Adel Merabet (M'10) received the Ph.D. in Engineering from Université du Québec à Chicoutimi, Canada, in 2007. He is an Associate Professor with the Division of Engineering, Saint Mary's University, Halifax, Canada. His research interests include renewable (wind-solar) energy conversion systems, energy management, advanced control systems and automation.



Khandker Tawfique Ahmed (M'14) received his B.Sc. degree in Electrical & Electronic Engineering from the Chittagong University of Engineering & Technology, Bangladesh in 2012. Currently he is pursuing M.Sc. in Applied Science at Saint Mary's University, Canada. His research interests are in distributed generation, renewable energy technologies, power system planning and control.



Hussein Ibrahim received the PhD in Engineering from Université du Québec à Chicoutimi, Canada. Since august 2009, he works as Scientific Manager at the TechnoCentre éolien, Gaspé, Canada. His research interests include wind energy, energy storage, hybrid energy systems, heat and mass transfer, fluid dynamics, energy efficiency.



Rachid Beguenane received the Ph.D. in electrical engineering from CNAM, Paris, France in 1994. He is an Associate Professor with the Department of Electrical & Computer Engineering, Royal Military College, Kingston, Canada. His research interests include renewable energy, real time simulation and FPGA.



Amer M.Y.M. Ghias (M'14) received the PhD degree in electrical engineering from the University of New South Wales, Australia, in 2014. He is an Assistant Professor at the Department of Electrical and Computer Engineering, University of Sharjah. His research interests include model predictive control of power electronics converter, hybrid energy storage, fault-tolerant converter, modulations and voltage balancing techniques for multilevel converter.